molecules

MDPI

Article

Vibronic and Cationic Features of 2-Fluorobenzonitrile and 3-Fluorobenzonitrile Studied by REMPI and MATI Spectroscopy and Franck–Condon Simulations

Shuxian Li [1], Yan Zhao [2,*], Yuechun Jiao [1,3], Jianming Zhao [1,3], Changyong Li [1,3,*] and Suotang Jia [1,3]

[1] State Key Laboratory of Quantum Optics and Quantum Optic Devices, Institute of Laser Spectroscopy, Shanxi University, Taiyuan 030006, China
[2] Department of Physics and Electronics Engineering, Jinzhong University, Jinzhong 030619, China
[3] Collaborative Innovation Center of Extreme Optics, Shanxi University, Taiyuan 030006, China
* Correspondence: zhaoy@jzxy.edu.cn (Y.Z.); lichyongl@sxu.edu.cn (C.L.)

Abstract: Fluorinated organic compounds have superior physicochemical properties than general organic compounds due to the strong C-F single bond; they are widely used in medicine, biology, pesticides, and materials science. In order to gain a deeper understanding of the physicochemical properties of fluorinated organic compounds, fluorinated aromatic compounds have been investigated by various spectroscopic techniques. 2-fluorobenzonitrile and 3-fluorobenzonitrile are important fine chemical intermediates and their excited state S_1 and cationic ground state D_0 vibrational features remain unknown. In this paper, we used two-color resonance two photon ionization (2-color REMPI) and mass analyzed threshold ionization (MATI) spectroscopy to study S_1 and D_0 state vibrational features of 2-fluorobenzonitrile and 3-fluorobenzonitrile. The precise excitation energy (band origin) and adiabatic ionization energy were determined to be 36,028 ± 2 cm^{-1} and 78,650 ± 5 cm^{-1} for 2-fluorobenzonitrile and 35,989 ± 2 cm^{-1} and 78,873 ± 5 cm^{-1} for 3-fluorobenzonitrile, respectively. The density functional theory (DFT) at the levels of RB3LYP/aug-cc-pvtz, TD-B3LYP/aug-cc-pvtz, and UB3LYP/aug-cc-pvtz were used to calculate the stable structures and vibrational frequencies for the ground state S_0, excited state S_1, and cationic ground state D_0, respectively. Franck–Condon spectral simulations for transitions of $S_1 \leftarrow S_0$ and $D_0 \leftarrow S_1$ were performed based on the above DFT calculations. The theoretical and experimental results were in good agreement. The observed vibrational features in S_1 and D_0 states were assigned according to the simulated spectra and the comparison with structurally similar molecules. Several experimental findings and molecular features were discussed in detail.

Keywords: fluorobenzonitrile; vibronic spectroscopy; cationic spectroscopy; MATI; Franck–Condon simulation

Citation: Li, S.; Zhao, Y.; Jiao, Y.; Zhao, J.; Li, C.; Jia, S. Vibronic and Cationic Features of 2-Fluorobenzonitrile and 3-Fluorobenzonitrile Studied by REMPI and MATI Spectroscopy and Franck–Condon Simulations. *Molecules* **2023**, *28*, 4702. https://doi.org/10.3390/molecules28124702

Academic Editor: Igor Reva

Received: 25 May 2023
Revised: 8 June 2023
Accepted: 9 June 2023
Published: 12 June 2023

1. Introduction

Due to the presence of the strong C-F single bond within the molecule, fluorinated organic compounds have superior physicochemical properties and are widely used in medicine, biology, pesticides, and materials science [1–5]. In recent years, a large number of fluorinated aromatic compounds have been investigated by various spectroscopic techniques. Ling et al. used femtosecond time-resolved photoelectron imaging to study the conformation of bi-fluorophenol and bi-fluoroaniline in the excited state S_1 after photoexcitation [6,7]. Wijngaarden's group used high-resolution microwave spectroscopy to measure the rotation spectra of fluorine substituted benzaldehyde, benzonitrile, phenol, and pyridine derivatives to study the molecular structure changes caused by fluorination and intramolecular hydrogen bonding interactions [8–10]. Many experimental groups have also studied the vibrational spectra of excited state S_1 and cationic ground state D_0 of fluorine-substituted phenol, anisole, and aniline derivatives using laser-induced fluorescence (LIF), resonance-enhanced multiphoton ionization (REMPI), and mass-analyzed

threshold ionization (MATI) spectroscopy [11–14]. Mono-fluorobenzonitrile is a very important class of intermediate for organic synthesis; its vibrational and rotational properties have been reported in many studies [15–18]. Kamaee et al. investigated the structural trends in mono-, di-, and pentafluorobenzonitriles using Fourier transform microwave spectroscopy [10]. Palmer et al. measured photoelectron spectroscopy of 2-fluorobenzonitrile (2FBN) and 3-fluorobenzonitrile (3FBN) and reported the ionization energies (IEs) of 9.78 eV and 9.79 eV, respectively [19]. Jiang and Levy used laser-induced fluorescence and dispersive fluorescence spectroscopy to study the vibrational relaxation of the excited state of 4-fluorobenzonitrile (4FBN) molecule [20]. In 2018, Zhao et al. [21] studied the vibrational features of the excited and cationic ground states of 4FBN by REMPI and MATI techniques. Silva et al. [16] measured the UV-Vis spectra of monofluorobenzonitriles in dichloromethane; from the curves they measured, the approximate origins of 2FBN and 3FBN could be estimated at 283 nm. To the best of our knowledge, the vibrational properties of the excited states and cationic ground states of 2FBN and 3FBN have not been reported in the literature.

MATI and zero kinetic energy (ZEKE) spectroscopy are currently the most popular high-resolution techniques for measuring vibrational features of cationic ground states. Kwon's group built a vacuum ultraviolet single photon MATI system to study many cationic vibrational features [22–29]. Tzeng's group and Ketkov's group used two-color MATI to study the cationic spectra of many benzene derivatives and sandwich molecules [30–36]. Wright's group used ZEKE technology to research cationic vibrational features of many halogenated benzene and their derivatives [37–42]. In this paper, we used two-color REMPI and MATI techniques to study the vibrational features of the excited states and cationic ground states of 2FBN and 3FBN. The precise excitation energies and adiabatic ionization energies were determined. The measured vibrational features were assigned and several experimental findings were analyzed and discussed in detail.

2. Results

The stable structures of 2- and 3-fluorobenzonitrile with atomic labels are shown in Figure 1. 2FBN and 3FBN molecules consist of 13 atoms with a total of 33 normal vibrational modes, 30 modes of which are at aromatic ring and 3 modes at CN group. The labeling convention of the vibrational modes followed the Varsanyi system [43]. Vibronic transitions were expressed in the Wilson notation based on the benzene modes, where the $v' \leftarrow v''$ transition in the normal mode n was represented by $n_{v''}^{v'}$ [44]; subscript V″ was omitted in the present research as it was a constant 0 (the low energy level of the transition is the vibrationless or zero point energy level of the low electronic state).

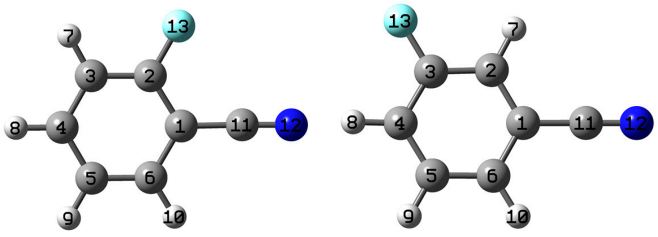

Figure 1. The stable structures of 2- and 3-fluorobenzonitrile with atomic labels.

2.1. Vibronic Features of 2-Fluorobenzonitrile in the S_1 State

The vibronic spectrum of the $S_1 \leftarrow S_0$ transition of 2FBN was measured by a two-color REMPI experiment with the vibration frequency range of 0–1350 cm^{-1}. The experimental result is shown in Figure 2a and its Franck–Condon simulation calculated at TD-B3LYP/aug-cc-pvtz level is shown in Figure 2b. It can be seen that the experimental result was in good agreement with the calculated one. The obvious feature of both REMPI and its simulation in Figure 2 was that the rate of signal-to-noise in the low frequency region was greater than in the high frequency region. The simulation spectrum showed that the bands in

the high frequency region were dense and consisted of many fundamentals, overtones, and combinations of various modes, many of which were very weak. Thus, dense and weak bands raised the spectral baseline and resulted in a bad rate of signal-to-noise in high frequency regions. The band at certain frequencies in the spectrum maybe came from several component (or vibration mode) contributions. For simplicity's sake, we only list the largest contributor in Table 1.

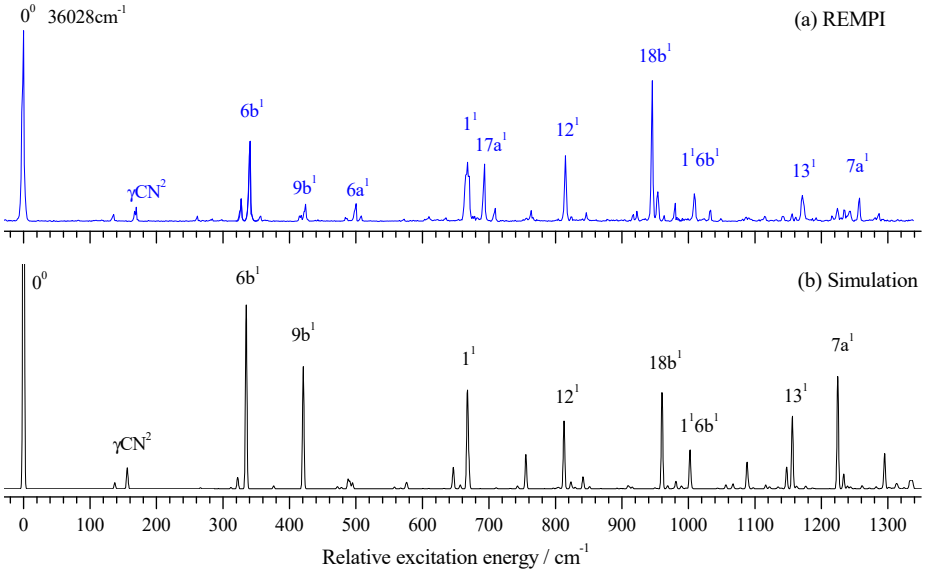

Figure 2. REMPI spectrum of 2-fluorobenzonitrile (**a**) and its Franck–Condon simulation (**b**).

Table 1. Observed bands in the vibronic spectrum of 2FBN and their possible assignments [a].

Transition Energy (cm^{-1})	Relative Intensity	Shift (cm^{-1})	Calc. (cm^{-1})	Assignment [b]
36,028	100	0	0	0^0
36,164	4	136	137	15^1
36,198	7	170	156	γCN^2
36,290	3	262		$10b^1\gamma CN^1$
36,356	12	328		$10a^1\gamma CN^1$
36,369	42	341	335	$6b^1$
36,452	9	424	421	$9b^1$
36,528	9	500	495	$6a^1$
36,638	3	610		$16a^110b^1$
36,663	31	635	646	$16b^2$
36,696	30	668	668	1^1
36,721	30	693	698	$17a^1$
36,738	7	710	711	$6b^110b^2$
36,792	6	764	755	$9b^16b^1$
36,843	34	815	813	12^1
36,874	2	846	841	$9b^2$
36,945	4	917	910	βCN^16b^1
36,950	5	922	916	$6a^19b^1$
36,974	74	946	960	$18b^1$
36,982	15	954	969	$12^1\gamma CN^2$
37,008	10	980	981	$6b^116b^2$
37,037	14	1009	1003	1^16b^1
37,062	6	1034	1022	$16b^210b^2$
37,199	14	1171	1156	13^1
37,285	12	1257	1224	$7a^1$
37,315	4	1287	1295	$18b^16b^1$

[a] Experimental values are shifts from 36,028 cm^{-1} and the calculated ones (scaled by 0.9649) are obtained from the TD-B3LYP/aug-cc-pvtz calculations. [b] β, in-plane bending; γ, out-of-plane bending.

Based on DFT calculation and spectral simulation, we analyzed and assigned the vibronic spectra of 2FBN. It is very clear in Figure 2a that the band at 36,028 cm^{-1} was assigned to the band origin of the $S_1 \leftarrow S_0$ transition. Many in-plane vibrational modes of the ring were active and most of them were very strong in the REMPI spectrum. The bands at 136, 341, 424, 500, 668, 815, 946, 1171, and 1257 cm^{-1} were assigned to fundamental modes 15, 6b, 9b, 6a, 1, 12, 18b, 13, and 7a, respectively. One out-of-plane fundamental mode at the ring was observed, which appeared at 693 cm^{-1} and was assigned to mode 17a. Several overtone vibrations were observed, which appeared at 170, 635, and 846 cm^{-1} and assigned to γCN^2, $16b^2$, and $9b^2$, respectively. Other bands observed in the REMPI spectrum were assigned to the combined vibrations of several modes. All the measured vibrational frequencies, calculated frequencies, and possible assignments are listed in Table 1.

From the measured REMPI spectra in Figure 2a, we found that the vibronic band 1^1 was much wider than other bands. From the simulation calculation, we knew that the band 1^1 consisted of three components: $16a^1 10a^1$ (665.2 cm^{-1}), 1^1 (667.5 cm^{-1}), and $6b^2$ (669.7 cm^{-1}). The calculated dipole strengths at the level of TD-B3LYP/aug-cc-pvtz for these three components were 3.365×10^{-5}, 1.254×10^{-2}, and 3.2×10^{-3}, respectively. Due to the very close vibrational energy, the resonance interactions may have played a role in the broadening of the experimental spectral line.

2.2. Photoionization Efficiency (PIE) Spectra of 2FBN

In order to measure the cationic spectra, we first required to know the ionization energy (IE). With the present experimental setup, the IE could be measured by photoionization efficiency (PIE) or MATI experiments. The PIE approach detected the prompt ions involving the field-ionization of high Rydberg neutrals and yielded a strong signal that led to an abruptly rising step near the ionization limit. In contrast, the MATI spectrum detected the threshold ions and yielded a sharp peak at the ionization threshold and vibrational features of the cation. We recorded both the PIE and MATI spectra by scanning the frequency of the ionization laser over a large range to determine the IE of 2FBN. Figure 3a,b show the PIE and MATI spectra via the intermediate state $S_1 0^0$ (36,028 cm^{-1}). The adiabatic IE of 2FBN was determined to be 78,647 ± 10 cm^{-1} by PIE and 78,650 ± 5 cm^{-1} (9.7514 ± 0.0006 eV) by MATI, including the correction of the Stark effect, respectively. These results were in good agreement with the previous measured value of 9.78 eV (78,881 cm^{-1}) [19] by photoelectron spectroscopy with an He I UV-light source.

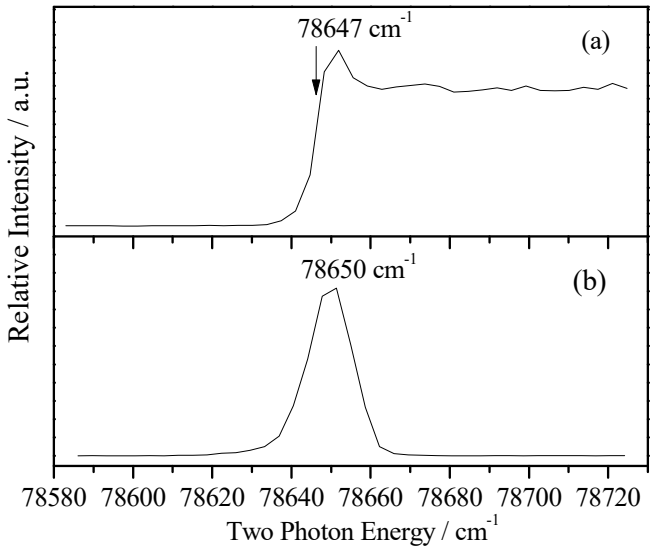

Figure 3. PIE spectrum of 2-fluorobenzonitrile recorded by ionizing via $S_1 0^0$ intermediate state at 36,028 cm^{-1} (**a**) and MATI spectrum near the cationic origin 0^+ for comparison (**b**).

2.3. Cationic Spectra of 2FBN

To investigate the molecular geometry and vibrational features of the 2FBN cation, the MATI spectra were recorded by ionizing via the $S_1 0^0$, $S_1 6b^1$ (0^0 + 341 cm^{-1}), $S_1 1^1$ (0^0 + 668 cm^{-1}), $S_1 12^1$ (0^0 + 815 cm^{-1}), and $S_1 18b^1$ (0^0 + 946 cm^{-1}) intermediate states.

We first performed the theoretical calculation and spectral simulation. The Franck–Condon simulation is shown in Figure 4a; the corresponding MATI spectrum via $S_1 0^0$ is shown in Figure 4b. From Figure 4a,b we know that the theoretical and experimental spectra were in good agreement. The most intense peak corresponded to the origin of the $D_0 \leftarrow S_1$ transition of 2FBN. Spectral features were assigned, mainly based on DFT calculations, the Franck–Condon simulation, and comparisons with the available data on substituted benzonitriles. Spectral assignment is a very tedious and error prone matter. Accurate assignments can be obtained by high dimensional or even full dimensional vibrational calculations [45,46]. For the present work, we used the Franck–Condon simulation, which greatly facilitated the spectral identification work. The bands at 131, 333, 530, 571, 683, 826, 972, 1268, and 1555 cm^{-1} were relatively intense and assigned to ring or CN group in-plane motion modes 15, 6b, 6a, βCN, 1, 12, 18b, 7a, and 8b, respectively. Several out-of-plane bending vibrations were also observed, such as γCN and 10b, appearing at 106 and 197 cm^{-1}, respectively. Other bands were weak and assigned to overtone or combination vibrations. The measured and calculated cationic vibrational frequencies and their possible assignments are listed in Table 2.

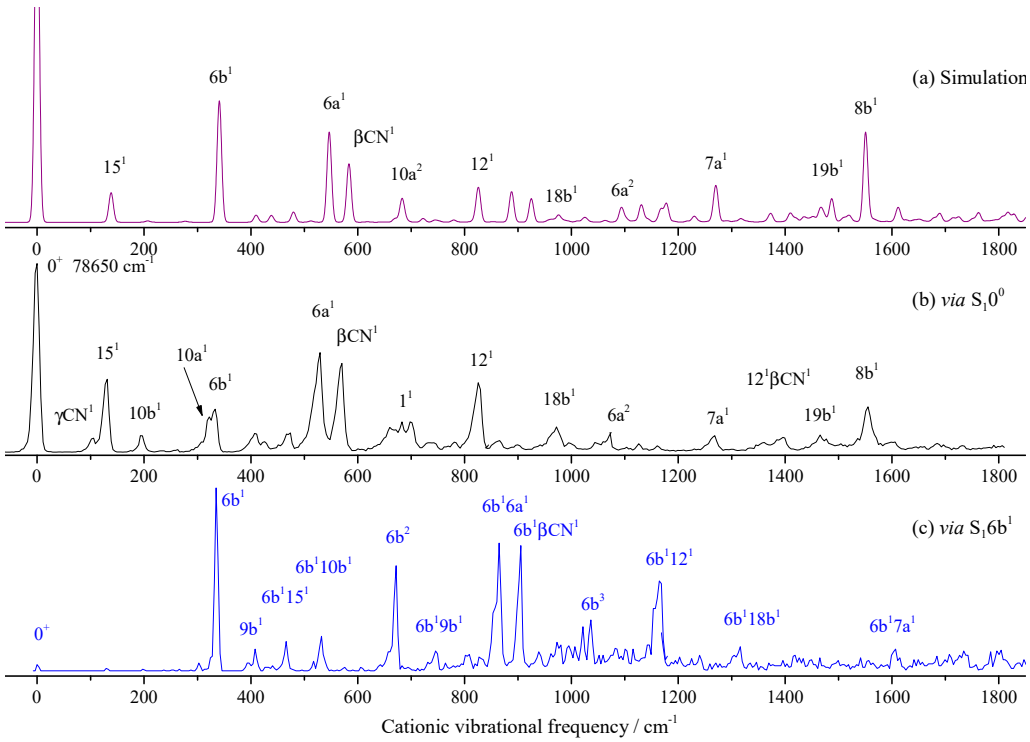

Figure 4. Franck–Condon simulation of the $D_0 \leftarrow S_1 0^0$ transition (**a**) and the MATI spectra of 2-fluorobenzonitrile *via* $S_1 0^0$ (**b**) and $S_1 6b^1$ (**c**) intermediate states.

In order to find more vibrational modes of 2FBN cation, the different intermediate states were used to record the MATI spectra. Figure 4c shows the MATI spectra *via* $S_1 6b^1$ (0^0 + 341 cm^{-1}). In comparison with Figure 4b, we found that, when $S_1 6b^1$ was used as the intermediate state, most of the spectral features could be assigned to combinations of 6b and the modes found in MATI via $S_1 0^0$. This could be verified by shifting Figure 4c to the left to align its band 6b with the 0^+ band in Figure 4b. No more fundamental modes than the MATI via $S_1 0^0$ were found.

Table 2. Assignment of the observed bands (cm^{-1}) in the MATI spectra of 2FBN [a].

Intermediate Levels in the S_1 State					Calc.	Assignment [b]
0^0	$6b^1$	1^1	12^1	$18b^1$		
106		106			104	γCN^1
131			130	132	139	15^1
197			193	199	205	$10b^1$
		209				γCN^2
		323	321	322	335	$10a^1$
333	335				341	$6b^1$
407	408		409	410	410	$9b^1$
		430				$6b^1\gamma CN^1$
	466					$6b^115^1$
474		473				$15^2\gamma CN^2$
		520				$10a^110b^1$
530			531	532	547	$6a^1$
	532					$6b^110b^1$
		582				$6b^115^1\gamma CN^1$
		643				$10a^2$
571			570	571	584	βCN^1
	672	672				$6b^2$
683		687		687	696	1^1
698						$16a^110b^1$
	746					$6b^19b^1$
		796				$1^1\gamma CN^1$
		818				1^115^1
826			823		826	12^1
	865					$6b^16a^1$
		888				1^110b^1
	906					$6b^1\beta CN^1$
		950				1^115^2
			955			12^115^1
972				973	976	$18b^1$
		1023				1^16b^1
	1036					$6b^3$
1059			1064			$6a^2$
				1104		$18b^115^1$
	1164		1160			$6b^112^1$
		1217				1^16a^1
1268					1271	$7a^1$
				1292		$18b^110a^1$
	1316			1321		$6b^118b^1$
		1329				1^110a^2

Table 2. *Cont.*

Intermediate Levels in the S_1 State					Calc.	Assignment [b]
0^0	$6b^1$	1^1	12^1	$18b^1$		
			1349			$12^1 6a^1$
			1394			$12^1 \beta CN^1$
1396					1410	$12^1 \beta CN^1$
1466					1466	$19b^1$
				1503		$18b^1 6a^1$
		1513				$1^1 12^1$
				1545		$18b^1 \beta CN^1$
1555					1551	$8b^1$
	1607					$6b^1 7a^1$
			1646			12^2

[a] The experimental values are shifts from 78,650 cm^{-1}, whereas the calculated ones are obtained from the B3LYP/aug-cc-pVDZ calculations, scaled by 0.9849. [b] β, in-plane bending; γ, out-of-plane bending.

Figure 5 shows the MATI spectra via the intermediate states of $S_1 1^1$ (0^0 + 668 cm^{-1}), $S_1 12^1$ (0^0 + 815 cm^{-1}), and $S_1 18b^1$ (0^0 + 946 cm^{-1}). Similarly, when $S_1 1^1$ (0^0 + 668 cm^{-1}) was used as the intermediate state, a lot of bands were assigned to the combination vibrations of the mode 1 and those found in MATI via $S_1 0^0$. In the lower frequency region, substituent CN out-of-plane bending γCN and its overtone γCN^2 were found. Aromatic ring out-of-plane bending 10a and its overtone $10a^2$ were also observed. Other bands were weak and were assigned to combination vibrations of several modes.

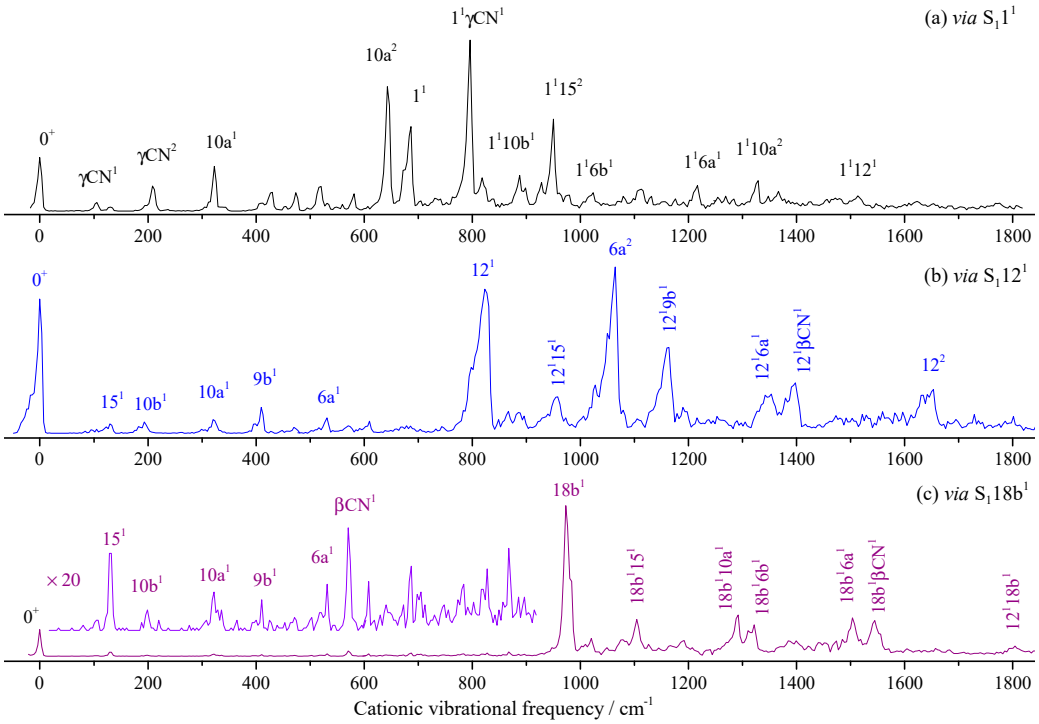

Figure 5. MATI spectra of 2-fluorobenzonitrile *via* $S_1 1^1$ (**a**), $S_1 12^1$ (**b**), and $S_1 18b^1$ (**c**) intermediate states.

Similarly, when $S_1 12^1$ was used as the intermediate, as shown in Figure 5b, except for the bands at 1064 and 1646 cm^{-1} being assigned to $6a^2$ and 12^2, other bands greater than 823 cm^{-1} ($D_0 12^1$) were assigned to combinations of 12^1 and other modes. In lower

frequency regions, some fundamental modes were active, which were found in the MATI spectrum via $S_1 0^0$ or $S_1 1^1$. For the MATI via $S_1 18b^1$ in Figure 5c, the spectral feature was similar to the MATI via $S_1 12^1$; all the assignments, as well as the calculated and measured values, are listed in Table 2.

2.4. Vibronic Features of 3-Fluorobenznitrile in the S_1 State

The vibronic spectrum in the S_1 state of 3FBN is shown in Figure 6a, together with its Franck–Condon simulation shown in Figure 6b for comparison. The entire simulated spectra appeared comparable to the 2-color REMPI spectra in Figure 6a. The distinct band corresponding to the transition energy of 35,989 cm^{-1} was identified as the origin of the $S_1 \leftarrow S_0$ electronic transition. Table 3 lists the observed vibronic transition energies, along with the energy shifts with respect to the band origin, band relative intensities, and possible assignments. The spectral assignment of 3FBN was accomplished by comparing with those of 4-fluorobenzonitrile, 3-fluorophenol, TD-B3LYP/aug-cc-pvtz calculation, and the Franck–Condon simulation. The spectral features in Figure 6a mainly resulted from vibronic transitions related to the in-plane ring deformation and substituent sensitive bending vibrations. The bands appearing at 140, 385, 401, 470, 560, 660, 958, 1147, 1271, and 1374 cm^{-1} were assigned to in-plane stretching or bending vibrations 15, 9a, 6b, 6a, βCN, 1, 12, 9b, 13, and 19a, respectively. The out-of-plane overtone vibrations $\gamma(CN)^2$ and $10b^2$ were also observed in lower frequency regions. Other bands were assigned to combination vibrations of several modes.

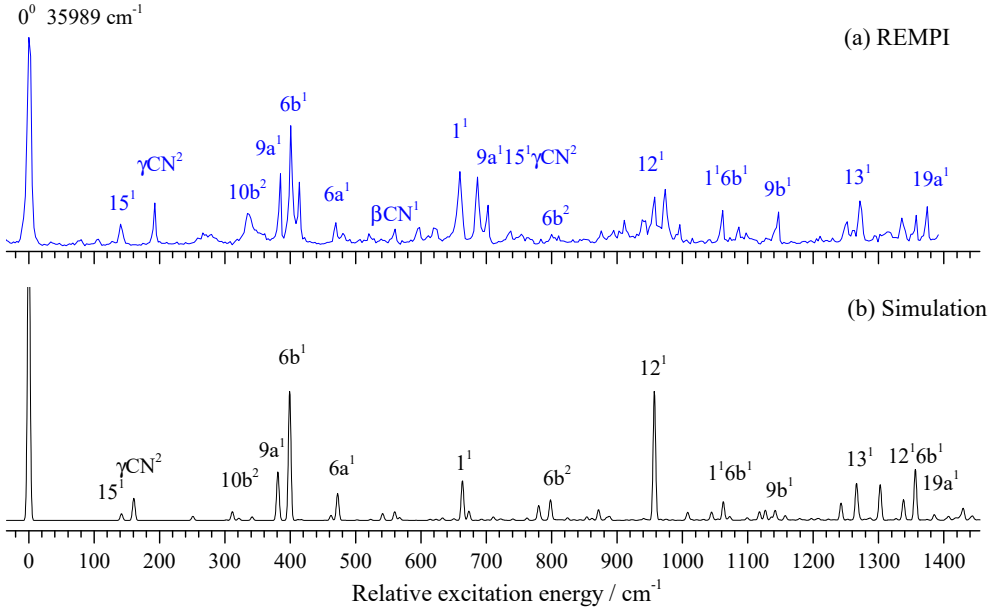

Figure 6. REMPI spectrum of 3-fluorobenzonitrile (**a**) and its Franck–Condon simulation (**b**).

Table 3. Assignment of observed bands (cm^{-1}) in the 2-color REMPI spectrum of 3FBN [a].

Transition Energy	Exp.	Relative Intensity	Calc. [a]	Assignment [b]
35,989	0	100		0^0, band origin
36,129	140	11	142	15^1
36,182	193	21	171	$\gamma(CN)^2$
36,255	266	7	251	$10b^1\gamma(CN)^1$
36,324	335	16	342	$10b^2$
36,374	385	35	381	$9a^1$, β(C-F)

Table 3. *Cont.*

Transition Energy	Exp.	Relative Intensity	Calc. [a]	Assignment [b]
36,390	401	58	399	$6b^1$, β(CCC)
36,403	414	31	417	$10b^1\gamma(CN)^3$
36,459	470	11	473	$6a^1$, β(CCC)
36,469	480	6	484	$10b^215^1$
36,509	520	6	523	$9a^115^1$
36,549	560	9	567	βCN
36,584	595	9	593	$10b^3\gamma(CN)^1$
36,611	622	9	623	$10a^2\gamma(CN)^2$
36,649	660	36	663	1^1, breather
36,675	686	33	684	$9a^115^1\gamma(CN)^2$
36,692	703	20	709	$15^1\beta(CN)^1$
36,727	738	8	741	$6b^110b^2$
36,789	800	6	798	$6b^2$
36,864	875	8	872	$6a^16b^1$
36,900	911	13	915	$1^110b^1\gamma(CN)^1$
36,927	938	13	940	$6b^215^1$
36,947	958	24	957	12^1
36,963	974	27	975	$1^110a^1\gamma(CN)^1$
36,985	996	11	996	$6a^19a^115^1$
37,051	1062	17	1063	1^16b^1
37,075	1086	9	1087	$4^16a^1\gamma(CN)^1$
37,136	1147	17	1142	$9b^1$
37,241	1252	12	1253	$6a^16b^19a^1$
37,260	1271	22	1266	13^1
37,304	1315	7	1314	$11^16b^116b^1$
37,324	1335	14	1338	12^19a^1
37,347	1358	15	1356	12^16b^1
37,363	1374	19	1385	$19a^1$

[a] The experimental values are shifts from 35,989 cm^{-1}, whereas the calculated ones are obtained from the TD-B3LYP/aug-cc-pVDZ calculations, scaled by 0.9722. [b] β, in-plane bending; γ, out-of-plane bending.

2.5. PIE Spectra of 3FBN

Similar to the 2FBN, ionization energy was very important for the cationic spectral measurements. We first performed the PIE experiment to determine the IE of 3FBN to be 78,873 ± 10 cm^{-1}. Then, we measured the MATI spectra to give the precise IE of 3FBN to be 78,873 ± 5 cm^{-1}. The PIE and MATI spectra via $S_1 0^0$ are shown in Figure 7a,b for comparison. It was obvious that they were very consistent.

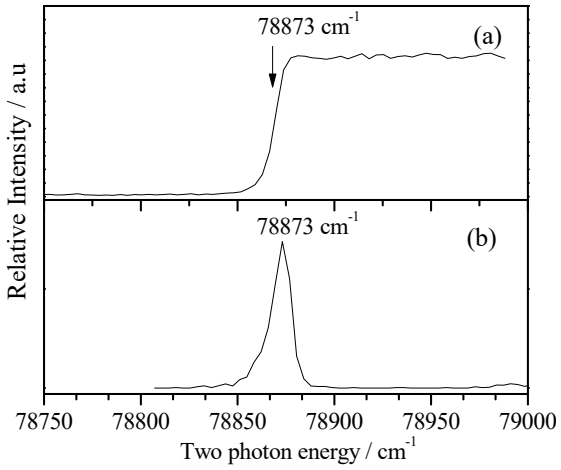

Figure 7. PIE spectrum of 3-fluorobenzonitrile recorded by ionizing via its $S_1 0^0$ state at 35,989 cm^{-1} (**a**) and MATI spectrum near the cationic origin 0^+ for comparison (**b**).

2.6. MATI Spectra of 3FBN

Figure 8a,b show the calculated Franck–Condon spectrum and measured MATI spectrum via $S_1 0^0$ state at 35,989 cm^{-1}, respectively. We can see that they were in good agreement. Many in-plane vibrations were active, such as modes 15, 6b, 6a, 1, 12, 18a, 9b, 18b, 13, and 8a appearing at 133, 371, 498, 668, 978, 1066, 1117, 1144, 1307, and 1566 cm^{-1}, respectively. Out-of-plane bending modes 10b and 10a were also observed, but they were weak. Other bands were assigned to combinations of several modes. All the experimental and calculated cationic vibrational frequencies of 3FBN and corresponding assignments are listed in Table 4.

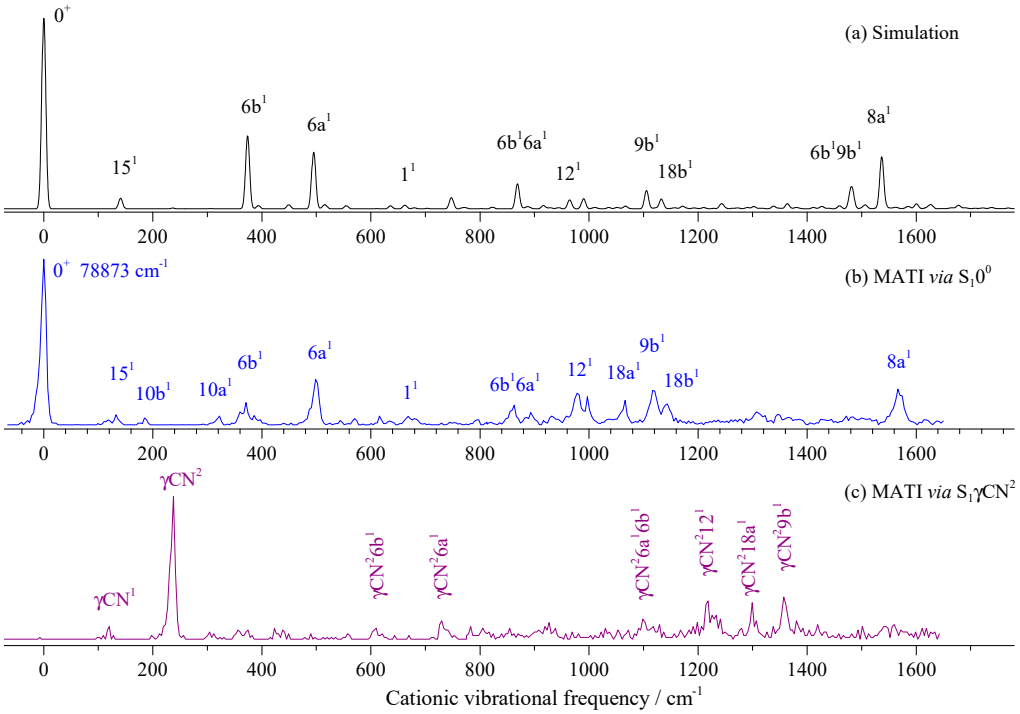

Figure 8. Franck–Condon simulation of the transition $D_0 \leftarrow S_1 0^0$ (**a**) and the MATI spectra of 3-fluorobenzonitrile *via* $S_1 0^0$ (**b**) and $S_1 \gamma CN^2$ (**c**) intermediate states.

Table 4. Assignment of observed bands (in cm^{-1}) in the MATI spectra of 3FBN [a].

Intermediate Levels in the S_1 State				Calc.	Assignment [b]
0^0	$\gamma(CN)^2$	$6b^1$	1^1		
	120			118	$\gamma(CN)^1$
133				141	15^1
	238			237	$\gamma(CN)^2$
185				188	$10b^1$
322				331	$10a^1$
371		370		374	$6b^1$, β(CCC)
		399		394	$9a^1$
498				495	$6a^1$, β(CCC)
		506			$6b^1 15^1$
	609				$\gamma(CN)^2 6b^1$
615				605	$16a^1$
668			668	679	1^1, breathing

Table 4. *Cont.*

Intermediate Levels in the S_1 State				Calc.	Assignment [b]
0^0	$\gamma(CN)^2$	$6b^1$	1^1		
		688			$6b^1 10b^1 15^1$
	730				$\gamma(CN)^2 6a^1$
		744			$6b^2$
			775		$4^1 10b^1$
			803		$1^1 15^1$
863		860			$6b^1 6a^1$
893		894			$6a^1 9a^1$
978				965	12^1, β(CCC)
997				990	$6a^2$
1066				1067	$18a^1$, β(CH)
	1098				$\gamma(CN)^2 6a^1 6b^1$
1117				1105	$9b^1$, β(CH)
1144				1133	$18b^1$, β(CH)
			1166		$1^1 6b^1$
	1218				$\gamma(CN)^2 12^1$
		1235			$6b^2 6a^1$
		1258			$6b^1 6a^1 9a^1$
	1299				$\gamma(CN)^2 18a^1$
1307				1302	13^1, β(CH)
		1350			$6b^1 12^1$
	1357				$\gamma(CN)^2 9b^1$
		1374			$6b^1 6a^2$
		1385		1382	$19a^1$
		1489			$6b^1 9b^1$
1566				1537	$8a^1$, ν(CC)
		1516			$6b^1 18b^1$
		1574			$6b^1 18a^1 15^1$

[a] The experimental values are shifts from 78,873 cm^{-1}, whereas the calculated ones are obtained from the B3LYP/aug-cc-pVDZ calculations, scaled by 0.9704. [b] β, in-plane bending; γ, out-of-plane bending.

When measuring the MATI via $S_1\gamma CN^2$ (Figure 8c), the distinct feature at 238 cm^{-1} was assigned to $D_0\gamma CN^2$, which followed the propensity rule $\Delta v = 0$. The fundamental vibration γCN^1 was also observed at 120 cm^{-1}, with a weak intensity, which did not appear in the REMPI spectrum. Other bands were assigned to combination vibrations of γCN^2 and fundamental vibrations.

When measuring the MATI via $S_1 6b^1$, as shown in Figure 9a, the distinct feature at 370 cm^{-1} was assigned to $D_0 6b^1$, which followed the propensity rule $\Delta v = 0$. The intense band at 399 cm^{-1} was assigned to $9a^1$. Other bands were assigned to combination vibrations of $6b^1$ and fundamental vibrations. Figure 9b shows the MATI spectrum via $S_1 1^1$, where the cationic vibration 1^1 (668 cm^{-1}) was most intense. The bands at 775, 803, and 1166 cm^{-1} were assigned to combination vibrations $4^1 10b^1$, $1^1 15^1$, and $1^1 6b^1$, respectively.

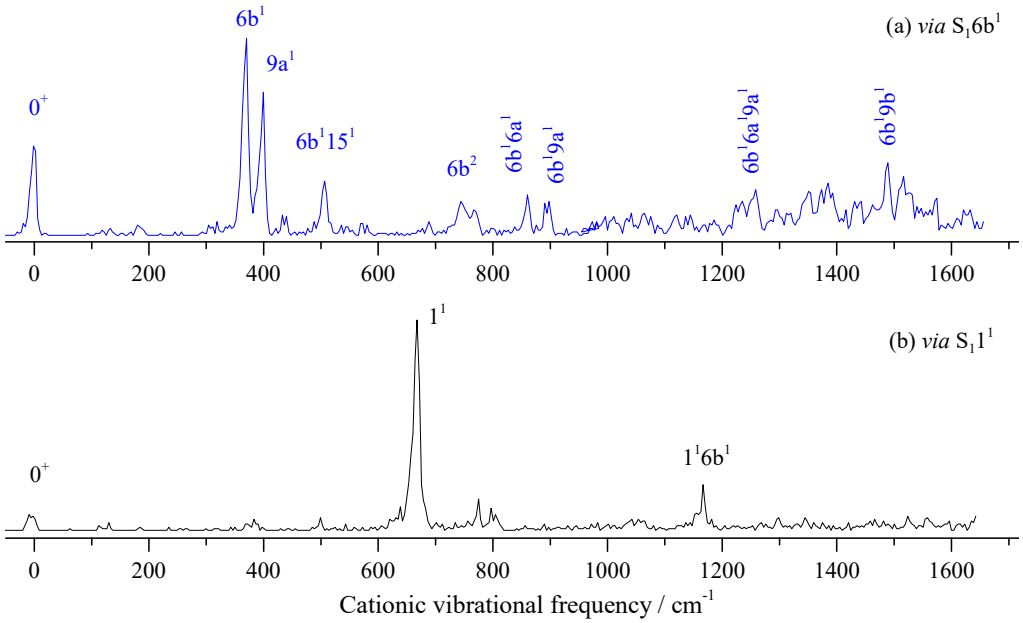

Figure 9. The MATI spectra of 3-fluorobenzonitrile *via* $S_1 6b^1$ (**a**) and $S_1 1^1$ (**b**) intermediate states.

3. Discussion

3.1. Breathing Vibrational Band of 2FBN

Whether the vibrational spectra of excited state S_1 or cationic ground state D_0, the frequencies of different vibrations in the high-frequency region may have been very close or even the same, which may have come from the fundamental, overtone, or combination vibrations. For example, the breathing vibration 1^1 of 2FBN in the REMPI spectrum (see Figure 2a) appeared at 668 cm^{-1}. The theoretical calculation showed that there were also two weaker vibrations $16a^1 10a^1$ and $6b^2$, whose vibrational frequencies were close to that of mode 1^1. The calculated vibration frequencies of $16a^1 10a^1$, 1^1, and $6b^2$ were 665.2 cm^{-1}, 667.5 cm^{-1} and 669.7 cm^{-1}, respectively. They were so close that the spaces between them were less than the experimental resolution, which led to a wide spectral band in the REMPI spectrum. When using this band as the intermediate state to perform the MATI experiment, according to the propensity rule of $\Delta v = 0$, these three vibrational modes of cation may be observed with great intensity. Generally, the vibration frequency of cation is slightly different from that of the excited state for the same vibrational mode and the frequency change can be not consistent for various vibration modes. So, these three vibration modes of cation of 2FBN may be separated in the MATI spectrum. As shown in Figure 5a, the cationic mode 1^1 appeared at 687 cm^{-1}, $6b^2$ appeared at 672 cm^{-1}, and $10a^1$ and $10a^2$ were also observed at 322.7 and 643.2 cm^{-1}, respectively. The strength of the MATI signal was not only related to the Franck–Condon factor but also to the population of the intermediate state S_1 and further related to the resonance degree of each vibration mode with the excitation ($S_1 \leftarrow S_0$) photon frequency. The experimental results demonstrated that the superposition band of several vibrations could be used as an intermediate state to perform the MATI experiments and more vibrational modes of cation could be observed.

3.2. Molecular Structure in S_0, S_1, and D_0 States and Vibrational Frequencies

Theoretical calculations showed that the stable configurations of the ground state S_0, excited state S_1, and cationic ground state D_0 of 2FBN and 3FBN molecules all had Cs symmetry and all the atoms were in the ring plane. This was consistent with their large Franck–Condon factors, intense REMPI and MATI signals, and MATI spectra, following the propensity rule of $\Delta v = 0$. However, in the transitions of $S_1 \leftarrow S_0$ and $D_0 \leftarrow S_1$, the bond length and bond angle of molecules changed slightly. Tables 5 and 6 show the bond lengths and bond angles of the S_0, S_1, and D_0 states of 2FBN and 3FBN calculated at levels of RB3LYP/ang-cc-pvtz, TD-B3LYP/ang-cc -pvtz, and UB3LYP/ang-cc-pvtz, respec-

tively. It can be seen that the bond lengths between adjacent carbon atoms of the ring of 2FBN were very close to the corresponding bond lengths of 3FBN. After the transition of $S_1 \leftarrow S_0$, each C−C bond length increased, resulting in the perimeters of ring of 2FBN and 3FBN increasing by 0.160 Å and 0.158 Å, respectively. The transition of $D_0 \leftarrow S_1$ led to the shortening of four C−C bonds and the lengthening of two C−C bonds. The overall effect of $D_0 \leftarrow S_1$ transition was that the perimeters of ring of 2FBN and 3FBN decreased by 0.073 Å and 0.072 Å, respectively. Further, the ring C−C bond lengths of D_0 state was averagely larger than that of S_0 state. The perimeters of the aromatic ring of 2FBN and 3FBN at the cationic ground states were 0.087 Å and 0.086 Å larger than those of the neutral ground state S_0, respectively. That is, the perimeters or average bond lengths of the ring in the ground state S_0, excited state S_1, and cationic ground state D_0 met the relationship: $S_0 < D_0 < S_1$. The length of a chemical bond reflects, to some extent, the strength of that bond. The greater the bond length, the weaker the bond strength. The frequency of an ideal oscillator is proportional to the square root of the bond strength, so the larger the bond length, the lower the vibration frequency. On this basis, we could predict that, on average, the vibration frequencies of the ground state S_0, the excited state S_1, and the cationic ground state D_0 met the relationship: $S_0 > D_0 > S_1$. The 33 normal vibration frequencies calculated at the B3LYP/ang-cc-pvtz level of 3FBN were statistically analyzed. On average, the vibration mode frequency of the ground state S_0 was about 21 cm^{-1} greater than that of the cationic ground state D_0 and the vibration frequency of D_0 was about 43 cm^{-1} greater than that of S_1. For example, the frequencies of breathing vibration mode 1 for S_0, D_0, and S_1 of 2FBN measured in the experiment were 724 [18], 685, and 668 cm^{-1}, respectively; for mode 12, they were 835 [18], 823, and 815 cm^{-1}, respectively; for mode 18b, they were 1100 [18], 973, and 946 cm^{-1}, respectively. The reported experimental and theoretical data of mFBT and mDFB [47] also indicated that most of the vibrational modes of these two molecules followed this rule. Furthermore, from the above vibration data, we know that the frequency variation was larger for the out-of-plane mode (such as 18b of 2FBN) than for the in-plane mode (such as modes 1 and 12 of 2FBN). Our DFT theoretical results showed that this law held for most vibration modes of benzene derivative.

Table 5. Bond length and bond angle of electronic ground state S_0, first excited state S_1, and cationic ground state D_0 of 2-fluorobenzonitrile calculated at RB3LYP/aug-cc-pvtz, TD-B3LYP/aug-cc-pvtz, and UB3LYP/aug-cc-pvtz levels, respectively.

	S_0	S_1	D_0	$\Delta(S_1 - S_0)$	$\Delta(D_0 - S_1)$	$\Delta(D_0 - S_0)$
Bond length (Å)						
C1−C2	1.396	1.436	1.455	0.040	0.019	0.059
C2−C3	1.381	1.406	1.393	0.025	−0.013	0.012
C3−C4	1.389	1.409	1.372	0.020	−0.037	−0.017
C4−C5	1.392	1.408	1.434	0.016	0.026	0.042
C5−C6	1.385	1.421	1.386	0.036	−0.035	0.001
C6−C1	1.401	1.424	1.391	0.023	−0.033	−0.010
C1−C11	1.427	1.395	1.407	−0.032	0.012	−0.020
C11−N12	1.152	1.165	1.158	0.013	−0.007	0.006
C2−F13	1.341	1.324	1.296	−0.017	−0.028	−0.045
Bond angle (°)						
C1−C2−C3	122.0	124.7	122.5	2.7	−2.2	0.5
C2−C3−C4	118.8	119.0	117.5	0.2	−1.5	−1.3
C3−C4−C5	120.5	118.1	121.1	−2.4	3.0	0.6
C4−C5−C6	120.0	122.7	121.4	2.7	−1.3	1.4
C5−C6−C1	120.4	120.6	119.0	0.2	−1.6	−1.4
C6−C1−C2	118.3	114.9	118.4	−3.4	3.5	0.1

Table 6. Bond length and bond angle of the electronic ground state S_0, first excited state S_1, and cationic ground state D_0 of 3-fluorobenzonitrile calculated at RB3LYP/aug-cc-pvtz, TD-B3LYP/aug-cc-pvtz, and UB3LYP/aug-cc-pvtz levels, respectively.

	S_0	S_1	D_0	$\Delta(S_1 - S_0)$	$\Delta(D_0 - S_1)$	$\Delta(D_0 - S_0)$
Bond length (Å)						
C1−C2	1.398	1.425	1.380	0.026	−0.045	−0.018
C2−C3	1.380	1.413	1.393	0.033	−0.019	0.013
C3−C4	1.384	1.406	1.433	0.022	0.027	0.049
C4−C5	1.390	1.404	1.374	0.014	−0.029	−0.016
C5−C6	1.387	1.411	1.395	0.024	−0.016	0.008
C6−C1	1.398	1.438	1.449	0.039	0.010	0.051
C1−C11	1.430	1.397	1.415	−0.033	0.017	−0.015
C11−N12	1.152	1.165	1.155	0.013	−0.009	0.003
C2−F13	1.346	1.330	1.300	−0.016	−0.030	−0.046
Bond angle (°)						
C1−C2−C3	118.2	118.4	116.9	0.2	−1.4	−1.3
C2−C3−C4	122.5	125.2	123.4	2.7	−1.7	0.9
C3−C4−C5	118.5	115.9	118.8	−2.6	2.9	0.3
C4−C5−C6	120.6	121.1	119.2	0.4	−1.9	−1.4
C5−C6−C1	119.6	122.2	120.9	2.6	−1.3	1.3
C6−C1−C2	120.4	116.9	120.5	−3.4	3.5	0.1

For 2FBN and 3FBN, the bond lengths of C−N in S_0 state were equal (1.152 Å), also equal in S_1 state (1.165 Å), and almost equal in D_0 state (1.158 and 1.155 Å). This means that the C−N bond was very strong and did not change with the substitution position (ortho- or meta-). The C−F bond length yielded a slight change, with different substitution positions.

The aromatic ring included six bond angles of C−C−C. In the electronic transition, the bond angle of the ring also underwent a certain degree of change. Four angles had a variation of approximately 2–3° and the other two had relatively small changes. In the transitions of $S_1 \leftarrow S_0$ and $D_0 \leftarrow S_1$, variations of the bond angle and bond length of rings led to the ring expansion and contraction, further activating a large number of in-plane vibration modes. Most of the observed vibronic features in the experiments were assigned to in-plane vibrations, only a few of out-of-plane modes were observed. Many benzene derivative molecules have exhibited such characteristics [48–53].

3.3. Substitution Effect on Ionization Energy

Molecular IE is an important parameter of molecular characteristics. In order to study the effect of fluorine and CN substitutions on ionization energy, we listed the IEs of benzene [54], fluorobenzene [55], benzonitrile [56], 2-fluorobenzonitrile, 3-fluorobenzonitrile, p-fluorobenzonitrile [21], phenol [57], o-fluorophenol [58], m-fluorophenol [59,60], and p-fluorophenol [11] in Table 7 and divided them into four groups for comparison. First, we found that three molecular IEs reduced with respect to their parent molecules, i.e., for the fluorine substitution, the ionization energy of fluorobenzene, 4-fluorophenol, and 4-fluorobenzonitrile was reduced by 330, 490, and 48 cm^{-1} compared with their parent molecules, respectively, where fluorine played a role of electron donor. However, fluorine-substituted ortho and meta benzonitrile slightly increased the IEs by 160 and 383 cm^{-1}, respectively; fluorine-substituted ortho and meta (cis and trans) phenols increased the IEs by 1381, 1563, and 1824 cm^{-1}, respectively. For these substitutions, fluorine exhibited electron withdrawing properties. It could be seen that the role of fluorine changed with the characteristics of the parent molecule and different substitution positions. Unlike fluorine substitution, CN-substituted benzene and fluorobenzene at ortho, meta, and para positions increased the ionization energy by 3933, 4423, 4646, and 3773 cm^{-1}, respectively, playing a role of strong electron withdrawing.

Table 7. Ionization energy of benzene and phenol and their F- and CN-substituted molecules (cm^{-1}).

Molecule	IE	ΔIE	Molecule	IE	ΔIE
Benzene [a]	74,557	0	Benzonitrile [c]	78,490	0
Fluorobenzene [b]	74,227	−330	2-Fluorobenzonitrile [d]	78,650	160
Benzonitrile [c]	78,490	3933	3-Fluorobenzonitrile [d]	78,873	383
			4-Fluorobenzonitrile [e]	78,000	−490
Phenol [f]	68,625	0			
2-Fluorophenol [g]	70,006	1381	Fluorobenzene [b]	74,227	0
3-Fluorophenol, cis [h,i]	70,188	1563	2-Fluorobenzonitrile [d]	78,650	4423
3-Fluorophenol, trans [h,i]	70,449	1824	3-Fluorobenzonitrile [d]	78,873	4646
4-Fluorophenol [j]	68,577	−48	4-Fluorobenzonitrile [e]	78,000	3773

[a] Ref. [54]. [b] Ref. [55]. [c] Ref. [56]. [d] This work. [e] Ref. [21]. [f] Ref. [57]. [g] Ref. [58]. [h] Refs. [59,60]. [i] Ref. [60]. [j] Ref. [11].

In addition, we can see from Table 7 that the effects of ortho and meta substitution on ionization energy were very close, while the effect of para substitution was relatively weak. Moreover, the IEs of molecules formed by ortho, meta, and para substitutions met the relative relationship: para < ortho < meta. Most benzene derivative molecules followed this rule.

4. Materials and Methods

4.1. Experimental Methods

The 2-fluorobenzonitrile and 3-fluorobenzonitrile samples were purchased from J&K Chemical and Sigma-Aldrich company, respectively. They were used without further purification. They were a colorless or a light brown liquid with a purity of 99%. The sample was heated to about 130 °C for 2FBN and 60 °C for 3FBN to obtain sufficient vapor pressure. Then, 3 bar krypton for 2FBN and 2.5 bar argon for 3FBN were used as the carrier gases; they carried the sample molecules into the beam source chamber through a pulse valve of 0.5 mm diameter nozzle (0.8 mm for 3FBN). Then, the molecule beam entered the ionization chamber through a skimmer located 20 mm downstream from the nozzle orifice. The vacuum pressures of the beam source and ionization chambers were ~4×10^{-4} Pa and ~6×10^{-6} Pa, respectively.

The light source consisted of two sets of dye lasers pumped by YAG lasers. One dye laser (CBR-D-24, Sirah) pumped by a frequency-tripled Nd: YAG laser (Qsmart 850, Quantel) was used as the excitation laser. Another dye laser (Precision Scan-D, Sirah) pumped by another frequency-tripled Nd: YAG laser (Qsmart 850, Quantel) was used as the ionization laser for two-color REMPI or probe laser for MATI experiments. The dyes of coumarin 540A and coumarin 460 or coumarin 480 were used for the excitation and ionization lasers, respectively. The dye laser wavelengths were calibrated by a wavemeter (WS7-60 UV-I). The fundamental outputs of the dye lasers were further frequency-doubled by BBO crystals.

Due to the strong electron-withdrawing ability of the CN group, the transition energies of $S_1 \leftarrow S_0$ were lower than those of $D_0 \leftarrow S_1$ for 2FBN and 3FBN. Such an energy structure indicated that two sets of light sources were required for the measurement of excited state spectra. In the REMPI experiments, we fixed the ionization laser at 232 nm, then scanned the excitation laser from 265 to 279 nm to obtain vibronic spectra of the first electronically excited state S_1 for 2FBN and 3FBN.

In the MATI experiments, the molecules in neutral ground state S_0 were resonantly excited to specific vibronic levels in the S_1 state, further excited to the high Rydberg state by the probe laser, which had a scanning range of 224–240 nm. A −0.5 V/cm pulsed electric field was applied to remove the prompt ions. After a time delay of about 29 μs, the Rydberg molecules were ionized by a 143 V/cm pulsed electric field. Newly formed threshold ions passed through a 48 cm field-free region to be detected by a microchannel plate (MCP) detector. The signal was collected by a multichannel scaler (SRS: SR430) and recorded by a

computer. Each mass spectrum was accumulated for 300 laser shots. The time sequence of the whole system was controlled by a pulse delay generator (SRS: DG645). More details on the experimental system have been described in our previous publications [61–63].

4.2. Theoretical Methods

All calculations were performed using the Gaussian 16 program package [64]. The geometry optimization and vibrational frequencies of S_0, S_1, and D_0 states were calculated at the levels of RB3LYP/aug-cc-pvtz, TD-B3LYP/aug-cc-pvtz, and UB3LYP/aug-cc-pvtz, respectively. Prior to the experiments, we also used the G4 and CBS-QB3 methods to predict IEs in order to select the appropriate dyes. The theoretical predicted adiabatic ionization energies (AIEs) by CBS-QB3 and G4 for 2FBN were 79,111 and 78,972 cm^{-1}, respectively, with relative errors of +0.59% and +0.41%. The predicted AIEs by CBS-QB3 and G4 for 3FBN were 79,480 and 79,043 cm^{-1}, respectively, with relative errors of +0.77% and +0.22%. The spectral simulations were performed based on the above B3LYP/aug-cc-pvtz calculations, which provided reliable accuracy. The broadening of the REMPI spectral lines was mainly caused by the Doppler effect, while the width of the MATI spectral lines was mainly caused by the ionization field applied to the Rydberg state. The Gaussian line shape, adiabatic Hessian, and time-independent model were used in constructing the spectra [65]. Combined with the theoretical calculations and simulated spectra, the vibrational features of 2FBN and 3FBN measured by the REMPI and MATI experiments were assigned.

5. Conclusions

The high-resolution vibrational spectra of the first electronically excited state S_1 and cationic ground state D_0 of 2-fluorobenzonitrile and 3-fluorobenzonitrile were measured by two-color resonance-enhanced multiphoton ionization and mass-analyzed threshold ionization spectroscopy. The precise band origins of $S_1 \leftarrow S_0$ transition and adiabatic ionization energies were determined to be 36,028 ± 2 cm^{-1} and 78,650 ± 5 cm^{-1} for 2-fluorobenzonitrile and 35,989 ± 2 cm^{-1} and 78,873 ± 5 cm^{-1} for 3-fluorobenzonitrile, respectively. DFT theory at the level of B3LYP/aug-cc-pvtz was used to calculate the molecular structure, vibrational frequency, and to further perform the Franck–Condon simulations. The theoretical results were in good agreement with the experimental measurements. The vibrational features of S_1 and D_0 states were analyzed in detail and assigned.

The MATI spectra followed well the propensity rule $\Delta\nu = 0$, indicating that the molecular structures of the cationic ground states were similar to that of the excited states. The molecular structures and vibration frequencies in S_0, S_1, and D_0 states were discussed in detail. The ring C-C bond lengths in S_0, S_1, and D_0 states averagely obeyed the rule of $S_1 > D_0 > S_0$. The bond length reflected the bond strength; further, the bond length was related to the vibration frequency. On average, or for most vibrational modes, the vibration frequencies of the ground state S_0, excited state S_1, and cationic ground state D_0 met the relative relationship: $S_1 < D_0 < S_0$. At the transition of $S_1 \leftarrow S_0$ and $D_0 \leftarrow S_1$, a lot of vibrational modes associated with ring in-plane distortion were active and only a few out-of-plane fundamental vibrations were observed. The substitution effects of F and CN were discussed. Whether the electron donating group or the electron withdrawing group, the ionization energies of molecules formed by ortho, meta, and para substitutions meet the relative relationship: para < ortho < meta.

Author Contributions: Conceptualization, C.L. and S.J.; investigation, S.L. and Y.Z.; writing—original draft preparation, C.L. and S.L.; writing—review and editing, C.L. and Y.Z.; funding acquisition, Y.J., J.Z. and S.J. All authors have read and agreed to the published version of the manuscript.

Funding: This research was funded by the National Natural Science Foundation of China (Grants Nos. 61835007, 12241408, 61575115), PCSIRT (Grant No. IRT_17R70), 111 project (Grant No. D18001), and the Fund for Shanxi "1331 Project" Key Subjects Construction.

Institutional Review Board Statement: Not applicable.

Informed Consent Statement: Not applicable.

Data Availability Statement: The data that support the findings of this study are available from the corresponding author upon reasonable request.

Conflicts of Interest: The authors declare no conflict of interest.

Sample Availability: Samples of 2-fluorobenzonitrile and 3-fluorobenzonitrile are available from commercial sources.

References

1. Berger, R.; Resnati, G.; Metrangolo, P.; Weber, E.; Hulliger, J. ChemInform Abstract: Organic Fluorine Compounds: A Great Opportunity for Enhanced Materials Properties. *ChemInform* **2011**, *42*, 3496–3508. [CrossRef]
2. Ametamey, S.M.; Honer, M.; Schubiger, P.A. Molecular imaging with PET. *Chem. Rev.* **2008**, *108*, 1501–1516. [CrossRef]
3. Müller, K.; Faeh, C.; Diederich, F. Fluorine in pharmaceuticals: Looking beyond intuition. *Science* **2007**, *317*, 1881–1886. [CrossRef]
4. Jeschke, P. The unique role of fluorine in the design of active ingredients for modern crop protection. *Chembiochem* **2004**, *5*, 571–589. [CrossRef]
5. Krüger, S.; Witte, F.; Helfrich, J.; Grotemeyer, J. Mass-analyzed-threshold-ionization (MATI) spectroscopy of 1,2,3-substituted halogenated benzenes via different intermediate vibrational states in the S_1 state. *RSC Adv.* **2015**, *5*, 937–948. [CrossRef]
6. Ling, F.; Li, S.; Song, X.; Tang, Y.; Wang, Y.; Zhang, B. Visualization of coherent nuclear motion between different geometries in photoexcited 2,4-difluorophenol. *Phys. Rev. A* **2017**, *95*, 043421. [CrossRef]
7. Ling, F.; Wang, Y.; Li, S.; Wei, J.; Tang, Y.; Zhang, B. Imaging Reversible and Irreversible Structural Evolution in Photoexcited 2,4-Difluoroaniline. *J. Phys. Chem. Lett.* **2018**, *9*, 5468–5473. [CrossRef]
8. Sun, W.; Lozada, I.B.; van Wijngaarden, J. Fourier Transform Microwave Spectroscopic and ab Initio Study of the Rotamers of 2-Fluorobenzaldehyde and 3-Fluorobenzaldehyde. *J. Phys. Chem. A* **2018**, *122*, 2060–2068. [CrossRef]
9. Sun, W.; van Wijngaarden, J. Structural elucidation of 2-fluorothiophenol from Fourier transform microwave spectra and ab initio calculations. *J. Mol. Struct.* **2017**, *1144*, 496–501. [CrossRef]
10. Kamaee, M.; Sun, M.; Luong, H.; van Wijngaarden, J. Investigation of Structural Trends in Mono-, Di-, and Pentafluorobenzonitriles Using Fourier Transform Microwave Spectroscopy. *J. Phys. Chem. A* **2015**, *119*, 10279–10292. [CrossRef]
11. Zhang, B.; Li, C.; Su, H.; Lin, J.L.; Tzeng, W.B. Mass analyzed threshold ionization spectroscopy of p-fluorophenol cation and the p-fluoro substitution effect. *Chem. Phys. Lett.* **2004**, *390*, 65–70. [CrossRef]
12. Huang, J.; Huang, K.; Liu, S.; Luo, Q.; Tzeng, W. Vibrational spectra and theoretical calculations of p-chlorophenol in the electronically excited S_1 and ionic ground D_0 states. *J. Photochem. Photobiol. A Chem.* **2008**, *193*, 245–253. [CrossRef]
13. Ratzer, C.; Nispel, M.; Schmitt, M. Structure of 4-fluorophenol and barrier to internal –OH rotation in the S_1-state. *Phys. Chem. Chem. Phys.* **2003**, *5*, 812–819. [CrossRef]
14. Zhang, L.; Liu, S.; Cheng, M.; Du, Y.; Zhu, Q. Vibrational Spectra and Theoretical Calculations of cis- and trans-3-Fluoro-N-methylaniline in the Neutral (S_0) and Cationic (D_0) Ground States. *J. Phys. Chem. A* **2016**, *120*, 81–94. [CrossRef]
15. Arivazhagan, M.; Meenakshi, R.; Prabhakaran, S. Vibrational spectroscopic investigations, first hyperpolarizability, HOMO-LUMO and NMR analyzes of p-fluorobenzonitrile. *Spectrochim. Acta A Mol. Biomol. Spectrosc.* **2013**, *102*, 59–65. [CrossRef]
16. Da Ribeiro Silva, M.A.V.; Monte, M.J.S.; Rocha, I.M.; Cimas, A. Energetic study applied to the knowledge of the structural and electronic properties of monofluorobenzonitriles. *J. Org. Chem.* **2012**, *77*, 4312–4322. [CrossRef]
17. Varadwaj, P.R.; Jaman, A.I. Centrifugal distortion analysis of the millimeter-wave spectrum of 2-fluorobenzonitrile and ab initio DFT calculations. *J. Mol. Spectrosc.* **2006**, *236*, 70–74. [CrossRef]
18. Kumar, A.P.; Rao, G.R. Vibrational analysis of substituted benzonitriles. I. Vibrational spectra, normal coordinate analysis and transferability of force constants of monohalogenated benzonitriles. *Spectrochim. Acta A Mol. Biomol. Spectrosc.* **1997**, *53A*, 2023–2032. [CrossRef]
19. Palmer, M.H.; Moyes, W.; Spiers, M. The electronic structure of substituted benzenes: Ab initio calculations and photoelectron spectra for benzonitrile, the tolunitriles, fluorobenzonitriles, dicyanobenzenes and ethynylbenzene. *J. Mol. Struct.* **1980**, *62*, 165–187. [CrossRef]
20. Jiang, S.; Levy, D.H. Supersonic Jet Studies on the Photophysics of Substituted Benzenes and Naphthalenes. *J. Phys. Chem. A* **2002**, *106*, 8590–8598. [CrossRef]
21. Zhao, Y.; Jin, Y.; Hao, J.; Yang, Y.; Li, C.; Jia, S. Resonance enhanced multiphoton ionization and mass analyzed threshold ionization spectroscopy of 4-fluorobenzonitrile. *Chem. Phys. Lett.* **2018**, *711*, 127–131. [CrossRef]
22. Eom, S.Y.; Lee, Y.R.; Kwon, C.H. Accurate conformational stability and cationic structure of piperidine determined by conformer-specific VUV-MATI spectroscopy. *Phys. Chem. Chem. Phys.* **2020**, *22*, 22823–22832. [CrossRef] [PubMed]
23. Park, S.M.; Lee, Y.R.; Kwon, C.H. Conformational Structures of Neutral and Cationic Pivaldehyde Revealed by IR-Resonant VUV-MATI Mass Spectroscopy. *Int. J. Mol. Sci.* **2022**, *23*, 14777. [CrossRef] [PubMed]
24. Lee, Y.R.; Kwon, C.H. Valence molecular orbitals and cationic structures of 2-fluoropyridine by high-resolution ion spectroscopy and Franck-Condon fitting. *J. Chem. Phys.* **2022**, *157*, 154306. [CrossRef]

25. Lee, Y.R.; Kwon, C.H. Innovative mass spectrometer for high-resolution ion spectroscopy. *J. Chem. Phys.* **2021**, *155*, 164203. [CrossRef]
26. Eom, S.Y.; Lee, Y.R.; Park, S.M.; Kwon, C.H. Determination of the highest occupied molecular orbital and conformational structures of morpholine based on its conformer-specific photoionization dynamics. *Phys. Chem. Chem. Phys.* **2022**, *24*, 28477–28485. [CrossRef]
27. Eom, S.Y.; Kang, D.W.; Kwon, C.H. Conformational structure of cationic tetrahydropyran by one-photon vacuum ultraviolet mass-analyzed threshold ionization spectroscopy. *Phys. Chem. Chem. Phys.* **2021**, *23*, 1414–1423. [CrossRef]
28. Lee, Y.R.; Kim, H.L.; Kwon, C.H. Determination of the cationic conformational structure of tetrahydrothiophene by one-photon MATI spectroscopy and Franck-Condon fitting. *Phys. Chem. Chem. Phys.* **2020**, *22*, 6184–6191. [CrossRef]
29. Kang, D.W.; Yoon, D.K.; Kwon, C.H. Conformational potential energy surfaces and cationic structure of 3,4-dihydro-2H-pyran by VUV-MATI spectroscopy and Franck-Condon fitting. *Phys. Chem. Chem. Phys.* **2020**, *22*, 27673–27680. [CrossRef]
30. Ketkov, S.Y.; Tzeng, S.-Y.; Rychagova, E.A.; Markin, G.V.; Makarov, S.G.; Tzeng, W.-B. Laser spectroscopic and computational insights into unexpected structural behaviours of sandwich complexes upon ionization. *Dalton Trans.* **2021**, *50*, 10729–10736. [CrossRef]
31. Ketkov, S.; Tzeng, S.-Y.; Rychagova, E.; Tzeng, W.-B. Ionization of Decamethylmanganocene: Insights from the DFT-Assisted Laser Spectroscopy. *Molecules* **2022**, *27*, 6226. [CrossRef] [PubMed]
32. Ketkov, S.Y.; Tzeng, S.Y.; Rychagova, E.A.; Kalakutskaya, L.V.; Fuss, M.; Braunschweig, H.; Tzeng, W.-B. Rydberg state mediated multiphoton ionization of (η^7-C_7H_7)(η^5-C_5H_5)Cr: DFT-supported experimental insights into the molecular and electronic structures of excited sandwich complexes. *Phys. Chem. Chem. Phys.* **2019**, *21*, 9665–9671. [CrossRef] [PubMed]
33. Ketkov, S.Y.; Rychagova, E.A.; Tzeng, S.-Y.; Tzeng, W.-B. TD DFT insights into unusual properties of excited sandwich complexes: Structural transformations and vibronic interactions in Rydberg-state bis(η6-benzene)chromium. *Phys. Chem. Chem. Phys.* **2018**, *20*, 23988–23997. [CrossRef] [PubMed]
34. Ketkov, S.Y.; Tzeng, S.-Y.; Wu, P.-Y.; Markin, G.V.; Tzeng, W.-B. DFT-Supported Threshold Ionization Study of Chromium Biphenyl Complexes: Unveiling the Mechanisms of Substituent Influence on Redox Properties of Sandwich Compounds. *Chemistry* **2017**, *23*, 13669–13675. [CrossRef] [PubMed]
35. Ketkov, S.Y.; Markin, G.V.; Tzeng, S.Y.; Tzeng, W.B. Fine Substituent Effects in Sandwich Complexes: A Threshold Ionization Study of Monosubstituted Chromium Bisarene Compounds. *Chemistry* **2016**, *22*, 4690–4694. [CrossRef]
36. Tzeng, S.Y.; Takahashi, K.; Tzeng, W.B. Two-Color Resonant Two-Photon Mass-Analyzed Threshold Ionization of 2,4-Difluoroanisole and the Additivity Relation of Ionization Energy. *J. Phys. Chem. A* **2020**, *124*, 10517–10526. [CrossRef]
37. Kemp, D.J.; Whalley, L.E.; Tuttle, W.D.; Gardner, A.M.; Speake, B.T.; Wright, T.G. Vibrations of the p-chlorofluorobenzene cation. *Phys. Chem. Chem. Phys.* **2018**, *20*, 12503–12516. [CrossRef]
38. Davies, A.R.; Kemp, D.J.; Wright, T.G. Electronic, vibrational, and torsional couplings in N-methylpyrrole: Ground, first excited, and cation states. *J. Chem. Phys.* **2021**, *154*, 224305. [CrossRef]
39. Kemp, D.J.; Gardner, A.M.; Tuttle, W.D.; Midgley, J.; Reid, K.L.; Wright, T.G. Identifying complex Fermi resonances in p-difluorobenzene using zero-electron-kinetic-energy (ZEKE) spectroscopy. *J. Chem. Phys.* **2018**, *149*, 094301. [CrossRef]
40. Davies, A.R.; Kemp, D.J.; Wright, T.G. Comment on "Electronic, vibrational and torsional couplings in N-methylpyrrole: Ground, first excited and cation states" [J. Chem. Phys. 154, 224305 (2021)]. *J. Chem. Phys.* **2021**, *155*, 117101. [CrossRef]
41. Kemp, D.J.; Fryer, E.F.; Davies, A.R.; Wright, T.G. Vibration-modified torsional potentials and vibration-torsion ("vibtor") levels in the m-fluorotoluene cation. *J. Chem. Phys.* **2019**, *151*, 084311. [CrossRef] [PubMed]
42. Davies, A.R.; Kemp, D.J.; Warner, L.G.; Fryer, E.F.; Rees, A.; Wright, T.G. Variations in Duschinsky rotations in m-fluorotoluene and m-chlorotoluene during excitation and ionization. *J. Chem. Phys.* **2020**, *152*, 214303. [CrossRef] [PubMed]
43. Varsányi, G. *Assignments for Vibrational Spectra of Seven Hundred Benzene Derivatives*; Adam Hilger: London, UK, 1974; ISBN 0852742835.
44. Wilson, E.B. The Normal Modes and Frequencies of Vibration of the Regular Plane Hexagon Model of the Benzene Molecule. *Phys. Rev.* **1934**, *45*, 706–714. [CrossRef]
45. Asmis, K.R.; Yang, Y.; Santambrogio, G.; Brümmer, M.; Roscioli, J.R.; McCunn, L.R.; Johnson, M.A.; Kühn, O. Gas-phase infrared spectroscopy and multidimensional quantum calculations of the protonated ammonia dimer $N_2H_7^+$. *Angew. Chem. Int. Ed. Engl.* **2007**, *46*, 8691–8694. [CrossRef]
46. Yang, Y.; Kuhn, O. A concise method for kinetic energy quantisation. *Mol. Phys.* **2008**, *106*, 2445–2457. [CrossRef]
47. Davies, A.R.; Kemp, D.J.; Wright, T.G. Unpicking vibration-vibration and vibration-torsion interactions in m-fluorotoluene. *J. Mol. Spectrosc.* **2021**, *381*, 111522. [CrossRef]
48. Zhang, L.; Yu, D.; Dong, C.; Cheng, M.; Hu, L.; Zhou, Z.; Du, Y.; Zhu, Q.; Zhang, C. Rotamers and isotopomers of 3-chloro-5-fluoroanisole studied by resonant two-photon ionization spectroscopy and theoretical calculations. *Spectrochim. Acta A Mol. Biomol. Spectrosc.* **2013**, *104*, 235–242. [CrossRef]
49. Xu, Y.; Tzeng, S.Y.; Shivatare, V.; Takahashi, K.; Zhang, B.; Tzeng, W.B. Identification of four rotamers of m-methoxystyrene by resonant two-photon ionization and mass analyzed threshold ionization spectroscopy. *J. Chem. Phys.* **2015**, *142*, 124314. [CrossRef]
50. Xu, Y.; Tzeng, S.Y.; Zhang, B.; Tzeng, W.B. Rotamers of 3,4-difluoroanisole studied by two-color resonant two-photon mass-analyzed threshold ionization spectroscopy. *Spectrochim. Acta A Mol. Biomol. Spectrosc.* **2013**, *102*, 365–370. [CrossRef]

51. Huang, W.C.; Huang, P.S.; Hu, C.H.; Tzeng, W.B. Vibronic and cation spectroscopy of 2,4-difluoroaniline. *Spectrochim. Acta A Mol. Biomol. Spectrosc.* **2012**, *93*, 176–179. [CrossRef]
52. Shivatare, V.S.; Kundu, A.; Patwari, G.N.; Tzeng, W.B. Studies of structural isomers o-, m-, and p-fluorophenylacetylene by two-color resonant two-photon mass-analyzed threshold ionization spectroscopy. *J. Phys. Chem. A* **2014**, *118*, 8277–8286. [CrossRef] [PubMed]
53. Li, C.; Lin, J.L.; Tzeng, W.B. Mass-analyzed threshold ionization spectroscopy of the rotamers of p-n-propylphenol cations and configuration effect. *J. Chem. Phys.* **2005**, *122*, 44311. [CrossRef] [PubMed]
54. Neuhauser, R.G.; Siglow, K.; Neusser, H.J. High n Rydberg spectroscopy of benzene: Dynamics, ionization energy and rotational constants of the cation. *J. Chem. Phys.* **1997**, *106*, 896–907. [CrossRef]
55. Lembach, G.; Brutschy, B. Fragmentation energetics and dynamics of fluorobenzene·Ar_n (n = 1–3) clusters studied by mass analyzed threshold ionization spectroscopy. *J. Chem. Phys.* **1997**, *107*, 6156–6165. [CrossRef]
56. Araki, M.; Sato, S.; Kimura, K. Two-Color Zero Kinetic Energy Photoelectron Spectra of Benzonitrile and Its van der Waals Complexes with Argon. Adiabatic Ionization Potentials and Cation Vibrational Frequencies. *J. Phys. Chem.* **1996**, *100*, 10542–10546. [CrossRef]
57. Dopfer, O.; Müller-Dethlefs, K. S1 excitation and zero kinetic energy spectra of partly deuterated 1:1 phenol–water complexes. *J. Chem. Phys.* **1994**, *101*, 8508–8516. [CrossRef]
58. Yuan, L.; Li, C.; Lin, J.L.; Yang, S.C.; Tzeng, W.B. Mass analyzed threshold ionization spectroscopy of o-fluorophenol and o-methoxyphenol cations and influence of the nature and relative location of substituents. *Chem. Phys.* **2006**, *323*, 429–438. [CrossRef]
59. Oikawa, A.; Abe, H.; Mikami, N.; Ito, M. Electronic spectra and ionization potentials of rotational isomers of several disubstituted benzenes. *Chem. Phys. Lett.* **1985**, *116*, 50–54. [CrossRef]
60. Yosida, K.; Suzuki, K.; Ishiuchi, S.; Sakai, M.; Fujii, M.; Dessent, C.E.H.; Müller-Dethlefs, K. The PFI-ZEKE photoelectron spectrum of m-fluorophenol and its aqueous complexes: Comparing intermolecular vibrations in rotational isomers. *Phys. Chem. Chem. Phys.* **2002**, *4*, 2534–2538. [CrossRef]
61. Zhao, Y.; Jin, Y.; Hao, J.; Yang, Y.; Wang, L.; Li, C.; Jia, S. Rotamers of p-isopropylphenol studied by hole-burning resonantly enhanced multiphoton ionization and mass analyzed threshold ionization spectroscopy. *Spectrochim. Acta A Mol. Biomol. Spectrosc.* **2019**, *207*, 328–336. [CrossRef]
62. Li, N.; Li, S.; Wang, L.; Wang, H.; Zhao, J.; Li, C. Vibrational spectra of 2-cyanophenol cation studied by the mass analyzed threshold ionization technique. *Chem. Phys. Lett.* **2022**, *792*, 139402. [CrossRef]
63. Hao, J.; Duan, C.; Yang, Y.; Li, C.; Jia, S. Resonance enhanced two-photon ionization and mass analyzed threshold ionization spectroscopy of 4-ethylanisole. *J. Mol. Spectrosc.* **2020**, *369*, 111258. [CrossRef]
64. Frisch, M.J.; Trucks, G.W.; Schlegel, H.B.; Scuseria, G.E.; Robb, M.A.; Cheeseman, J.R.; Scalmani, G.; Barone, V.; Mennucci, B.; Petersson, G.A.; et al. *Gaussian 16 Revision C.01*; Gaussian Inc.: Wallingford, CT, USA, 2016.
65. Baiardi, A.; Bloino, J.; Barone, V. General Time Dependent Approach to Vibronic Spectroscopy Including Franck-Condon, Herzberg-Teller, and Duschinsky Effects. *J. Chem. Theory Comput.* **2013**, *9*, 4097–4115. [CrossRef] [PubMed]